MATHEMATICAL BIOSCIENCES
AND ENGINEERING
Volume **11**, Number **5**, October **2014**

doi:10.3934/mbe.2014.11.1199

pp. **1199–1214**

EFFECT OF RESIDUAL STRESS ON PEAK CAP STRESS IN ARTERIES

Rebecca Vandiver

St. Olaf College
1520 St. Olaf Ave
Northfield, MN 55057, USA

(Communicated by Qing Nie)

Abstract. Vulnerable plaques are a subset of atherosclerotic plaques that are prone to rupture when high stresses occur in the cap. The roles of residual stress, plaque morphology, and cap stiffness on the cap stress are not completely understood. Here, arteries are modeled within the framework of nonlinear elasticity as incompressible cylindrical structures that are residually stressed through differential growth. These structures are assumed to have a nonlinear, anisotropic, hyperelastic response to stresses in the media and adventitia layers and an isotropic response in the intima and necrotic layers. The effect of differential growth on the peak stress is explored in a simple, concentric geometry and it is shown that axial differential growth decreases the peak stress in the inner layer. Furthermore, morphological risk factors are explored. The peak stress in residually stressed cylinders is not greatly affected by changing the thickness of the intima. The thickness of the necrotic layer is shown to be the most important morphological feature that affects the peak stress in a residually stressed vessel.

1. **Introduction.** Over time, coronary arteries can develop atherosclerosis, characterized by local thickening of the vessel wall. A subset of atherosclerotic plaques, called vulnerable plaques, are particularly unstable and prone to rupture. When rupture occurs, platelets collect at the site of the injury and these can form clots large enough to block the artery. Vulnerable plaques are characterized by a thin fibrous cap and a large lipid-rich necrotic core. The wall shear stress ($< 10^{-2}$ kPa) due to blood flow ([16]), is extremely low compared to the critical stress within the plaque (300 kPa) ([34], [17]). Therefore, the structural stress in plaques plays an important role in plaque rupture ([34], [32].

Computational studies have been done to study stress in vulnerable plaques and to understand morphological risk factors for rupture. Studies have shown that stresses in the cap increase with decreasing cap thickness ([6], [33], [19]). [24] showed that the size of the necrotic core has a significant influence on cap stresses. Finite element analyses performed by [2] showed that cap thickness was the most important morphological risk factor for stiff intima models but the necrotic core thickness and necrotic core angle have a larger impact in soft intima models. However, residual stresses were not included in these models. [23] showed that residual stresses

2010 *Mathematics Subject Classification.* Primary: 92C10; Secondary: 74A10.

Key words and phrases. Atherosclerosis, morphoelasticity, residual stress, nonlinear elasticity, anisotropic.

have been shown to be non-negligible in vulnerable plaques and that residual stress dramatically affects the physiological peak stress amplitude in the thin fibrous cap. This study also showed that residual stress does not shift the peak stress within the cap. However, a full three-dimensional morphoelastic model that includes axial residual stress is needed in order to understand the full effects of residual stress.

Residual stresses in arteries, and many other biological materials, are known to be the result of differential growth, that is different parts of the tissue grow at different rates. The existence of residual stress in arteries ([18], [35], [35], [30]) has been demonstrated by performing radial cuts on unloaded rings. Thin rings of each of these tissues will open up into sectors, indicating the presence of internal stresses in the intact structures. Furthermore, axial strips of the different layers of the arteries will compress or extend when separated.

For a healthy, young artery, [9] showed that the intima contributes negligible mechanical strength to the arterial wall. Therefore, morphoelastic models have focused on two-layer models incorporating the media/intima and the adventitia ([30], [7], [29]). However, for aged human arteries the intima exhibits considerable thickness and strength. Previous morphoelastic models have not taken into account the intima or necrotic components.

The purpose of this article is to study theoretically the mechanical effect of residual stresses in an artery with intimal thickening that includes a low stiffness layer representing the necrotic layer. Previous studies have used two-dimensional models ([23]) and neglected to include residual stresses ([6], [2], [33], [19]) in their computations. Therefore this work is novel in that a residually stressed three-dimensional morphoelastic model is used to understand the full effects of residual stress. While vulnerable plaques tend to be asymmetric ([21]), here we focus on concentric lesions to first understand the effects of residual stress in a simpler geometry. The media and adventitia are assumed to be anisotropic hyperelastic materials proposed by [10] while the intima and necrotic layers are modeled as isotropic neo-Hookean materials due to the fact that little is known regarding the mechanical effects of the atherosclerotic intima. Residual stress is introduced through a multiplicative decomposition of the growth tensor as proposed by [28]. These tools are used to answer the following questions:

1. What is the effect of residual stress on the peak stress in an artery?
2. What is the influence of morphological features such as the thicknesses of the intima and necrotic layers in a residually stressed artery?
3. How does the stiffness of the intima affect the peak stress in a residually stressed artery?

2. **A mechanical model of growing arteries.**

2.1. **Kinematics.** Consider a continuous body whose reference configuration is defined by $\mathcal{B}_0$ (see Figure 1). Let $\mathbf{X}$ denote the position vectors in $\mathcal{B}_0$. The body is deformed to the new current configuration, $\mathcal{B}_f$ where the position of a material point $\mathbf{X}$ is $\mathbf{x} = \boldsymbol{\chi}(\mathbf{X}, t)$. The deformation gradient, $\mathbf{F}(\mathbf{X}, t) = \text{Grad}\boldsymbol{\chi}$ relates a material segment in the reference configuration to the same segment in the current configuration. Here, we use the fundamental assumption of morphoelasticity that follows from early work in elastoplasticity ([13], [25]) and was first described in [26]. It states that the deformation gradient $\mathbf{F}(\mathbf{X}, t)$ can be decomposed into a product of a growth tensor $\mathbf{G}(\mathbf{X}, t)$ and an elastic tensor $\mathbf{A}(\mathbf{X}, t)$, so that

$$\mathbf{F}(\mathbf{X},t) = \mathbf{A}(\mathbf{X},t)\cdot\mathbf{G}(\mathbf{X},t). \tag{1}$$

As shown in Figure 1, the growth tensor $\mathbf{G}(\mathbf{X},t)$ maps $\mathcal{B}_0$ to the virtual configuration $\mathcal{V}$ which is locally stress-free. The growth deformation tensor may not result in a continuous change from point to point and may not be compatible. If we require continuity of the body, the elastic deformation is introduced which in turn causes residual stress in the grown body $\mathcal{B}_f$.

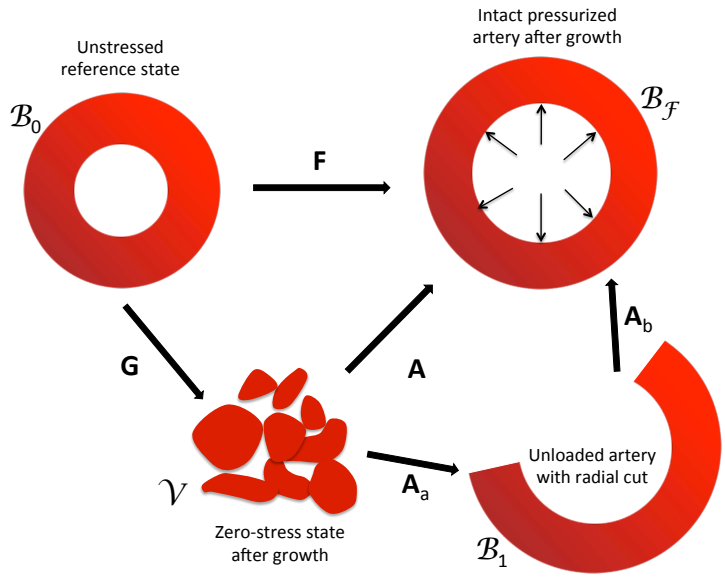

FIGURE 1. Decomposition of a growing, pressurized body.

2.2. **Mechanical equilibrium.** We now consider the balance of forces acting on $\mathcal{B}_f$. Balancing linear momentum and using Cauchy's theorem, the equation for mechanical equilibrium is given by

$$\operatorname{div}(\mathbf{T}^{\mathrm{T}}) = 0, \qquad \mathbf{T}^{\mathrm{T}} = \mathbf{T}, \tag{2}$$

where the divergence is taken with respect to $\mathbf{x}$ in the current configuration. The solutions to the equilibrium equations must also satisfy the dead-loading conditions imposed on the boundary. The artery is assumed to have zero pressure on the outer wall and a constant internal pressure mimicking the systolic blood pressure experienced by the arterial wall in vivo.

We assume that the body is hyperelastic. That is, the material can be described by a strain energy function $W = W(\mathbf{A})$. Assuming the material is incompressible, the Cauchy stress is related to the elastic deformation, $\mathbf{A}$, by

$$\mathbf{T} = \mathbf{A}\cdot\frac{\partial W}{\partial \mathbf{A}} - p\mathbf{I}, \tag{3}$$

where p is a Lagrange multiplier associated with the internal constraint of incompressibility.

2.3. **Elastic response.** The model we consider is a five-layered model with an inner intima layer, necrotic layer (low stiffness layer), outer intima layer, media, and adventitia. In a healthy artery, [9] showed that the intima is known to have negligible (solid) mechanical contributions. However, in an artery with intimal thickening, the intima is a relevant layer with significant load-bearing capacity ([11], [27]). The composition of plaques can vary greatly and therefore the mechanical properties can be highly variable. The intima and necrotic layers are assumed to be neo-Hookean ([8]) with the strain energy density function given by

$$W = C(I_1 - 3) \tag{4}$$

where $I_1 = \alpha_r^2 + \alpha_\theta^2 + \alpha_z^2$ is an invariant of the right Cauchy-Green tensor $\mathbf{C} = \mathbf{F}^T \cdot \mathbf{F}$ and C is a material constant in units [N/m^2]. For small deformations, C can be derived form the Young's modulus, E, by $C = E/6$. The necrotic core is assumed to be a very soft tissue ($E = 1$ kPa) ([20]). Experimental studies on atherosclerotic plaque material properties have reported E values from 33 kPa to 1000 kPa ([4], [15], [3], [14]). An intermediate stiffness ($E = 500$) will be used for the intima but we will also show results for low ($E = 100$) and high ($E = 1000$) values to test how sensitive the results are to this parameter.

Numerous constitutive models have been proposed for the media and adventitia layers of arteries (see review in [12]). Here, we use a structural model introduced by [11] for coronary arteries with intimal thickening. The media and adventitia tissue are known to be anisotropic due to the fact that each layer is reinforced with collagen fibers with preferred directions. The model accounts for the orientations of the collagen fibers in each layer. The contribution of collagen fibers in the arterial wall is considered to be negligible at low pressures and therefore, the mechanical response is assumed to be isotropic. However, at higher pressures, the collagen fibers are stretched and the resulting mechanical response is anisotropic. For the media and adventitia, the strain energy density function is given by

$$W = \mu(I_1 - 3) + \frac{k_2}{k_1}\left(\exp\{k2\left[(1-\rho)(I_1-3)^2 + \rho(I_4-1)^2\right]\} - 1\right) \tag{5}$$

where $\mu > 0$ and $k_1 > 0$ are stress like parameters, $k_2 > 0$ and $\rho \in [0, 1]$ are dimensionless parameters, and $I_4 > 1$ is an invariant of the right Cauchy-Green tensor. The invariant $I_4 = \lambda_\theta^2 \cos^2\phi_j + \lambda_z^2 \sin^2\phi_j$ is the square of the stretch in the direction of the two families of collagen fibers. The two families of (collagen) fibers are arranged in symmetrical spirals, here assumed to be mechanically equivalent. The fibers are assumed to be embedded in the tangential surface of the tissue where ϕ_j represents the angle between the fibers. The subscript $j = m, a$ refers to the media and adventitia. Parameter values are taken from [11] for a coronary artery: $k_{1m} = 21.60, k_{2m} = 8.21, k_{1_a} = 38.57, k_{2a} = 85.03, \phi_m = 20.61°, \phi_a = 67°, \rho_m = 0.25, \rho_a = 0.55$.

2.4. **Growth formulation.** For the particular case of an artery with intimal thickening and a necrotic layer within the intima, we consider a five-layered cylinder with an inner intima layer of initial radii A and A_1, necrotic layer of initial radii A_1 and A_2, outer intima layer of initial radii A_2 and B, media of initial radii B and C, and adventitia of initial radii C and D (shown in Figure 2). We consider a finite deformation in which the cylinder is allowed to grow and deform while remaining cylindrical. Unlike eccentric plaques, bending generally does not occur in concentric

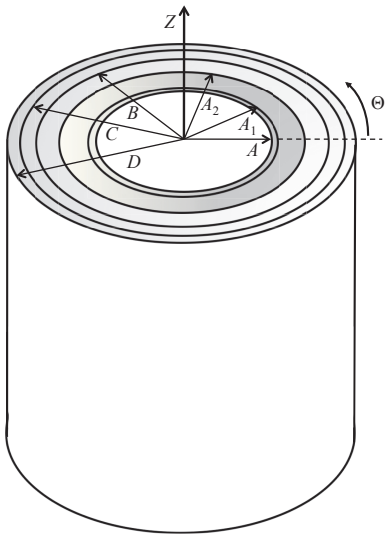

FIGURE 2. Geometry in the initial configuration. The intima has initial and outer radii of A and B with a low stiffness layer (necrotic layer) between A_1 and A_2. The media has initial inner and outer radii B and C and the adventitia is between C and D.

plaques [5]. The finite deformation of each cylindrical shell is given by

$$\mathbf{x} = \boldsymbol{\chi}(\mathbf{X}, t), \tag{6}$$

and

$$\mathbf{X} = (R, \Theta, Z), \qquad \mathbf{x} = (r, \theta, z), \tag{7}$$

$$r = r(R), \quad \theta = \Theta, \quad z = \lambda Z \tag{8}$$

The geometric deformation in cylindrical coordinates is

$$\mathbf{F} = \text{Grad}(\boldsymbol{\chi}) \tag{9}$$

$$= \text{diag}(r', r/R, \lambda), \tag{10}$$

where the gradient is take in the reference configuration, the prime denotes differentiation with respect to R, and λ is the axial stretch of the cylinder. The growth tensor is given by

$$\mathbf{G} = \text{diag}(\gamma_r, \gamma_\theta, \gamma_z). \tag{11}$$

where γ_r, γ_θ and γ_z are the dimensionless geometric stretch factors associated with growth in the radial, circumferential and axial directions, respectively. The values of these growth stretch factors will be determined from known values of the residual strain in Section 2.6. The elastic tensor is given by

$$\mathbf{A} = \text{diag}\left(\frac{\gamma_z}{\alpha\lambda}, \alpha, \frac{\lambda}{\gamma_z}\right) \tag{12}$$

where we have used the incompressibility condition $\det\mathbf{A} = 1$ and $\alpha = r/(R\gamma_\theta)$. The decomposition $\mathbf{F} = \mathbf{A}\cdot\mathbf{G}$ together with the incompressibility condition implies $\det\mathbf{F} = \det\mathbf{G}$. Therefore the function $r(R)$ in Equation 8 satisfies

$$\frac{dr}{dR} = \frac{\gamma_r\gamma_\theta\gamma_z R}{r\lambda} \tag{13}$$

At the interfaces separating different layers, the displacements must be continuous, that is

$$r(a_1^+) = r(a_1^-), \quad r(a_2^+) = r(a_2^-), \quad r(b^+) = r(b^-), \quad r(c^+) = r(c^-). \tag{14}$$

2.5. **Finite deformation.** Assuming that in the deformation the cylinder retains its cylindrical symmetry, the only non-vanishing equation in the mechanical equilibrium Equation (2) is

$$\frac{\partial T_{rr}}{\partial r} + \frac{T_{rr} - T_{\theta\theta}}{r} = 0. \tag{15}$$

where the Cauchy stress tensor is given by $\mathbf{T}$= diag$(T_{rr}, T_{\theta\theta}, T_{zz})$. Using the auxiliary function $\hat{W}(\alpha) = W(\gamma_z/(\alpha\lambda), \alpha, \lambda/\gamma_z)$, the stress-strain relationship in (3) can be used in the mechanical equilibrium Equation (2) to obtain

$$\frac{\partial T_{rr}(r)}{\partial r} = \begin{cases} \frac{\alpha\partial_\alpha\hat{W}^{(i1)}}{r} & a \le r \le a_1, \\ \frac{\alpha\partial_\alpha\hat{W}^{(n)}}{r} & a_1 \le r \le a_2, \\ \frac{\alpha\partial_\alpha\hat{W}^{(i2)}}{r} & a_2 \le r \le b, \\ \frac{\alpha\partial_\alpha\hat{W}^{(m)}}{r} & b \le r \le c, \\ \frac{\alpha\partial_\alpha\hat{W}^{(a)}}{r} & c \le r \le d, \end{cases} \tag{16}$$

where the superscripts $i1, n, i2, m, a$ refer to the inner intima, necrotic layer, outer intima, media, and adventitia layers, respectively. Assuming the boundary conditions of zero normal traction on the outer boundary and an internal pressure, P, at the inner boundary ($T_{rr}(a) = -P$ and $T_{rr}(d) = 0$), we integrate Equation (16) to obtain an equation for the radial stress

$$T_{rr}(r) = \begin{cases} -P + \int_a^r \frac{\alpha\partial_\alpha\hat{W}^{(i1)}}{r'}dr' & a \le r \le a_1, \\ T_{rr}(a_2) - \int_r^{a_2} \frac{\alpha\partial_\alpha\hat{W}^{(n)}}{r'}dr' & a_1 \le r \le a_2, \\ T_{rr}(b) - \int_r^{b} \frac{\alpha\partial_\alpha\hat{W}^{(i2)}}{r'}dr' & a_2 \le r \le b, \\ T_{rr}(c) - \int_r^{c} \frac{\alpha\partial_\alpha\hat{W}^{(m)}}{r'}dr' & b \le r \le c, \\ -\int_r^{d} \frac{\alpha\partial_\alpha\hat{W}^{(a)}}{r'}dr' & c \le r \le d. \end{cases} \tag{17}$$

The hoop stress and axial stress are given by

$$T_{\theta\theta}(r) = T_{rr} + \alpha W_2 - \frac{\gamma_z}{\lambda\alpha}W_1, \qquad T_{zz}(r) = T_{rr} + \frac{\lambda}{\gamma_z}W_3 - \frac{\gamma_z}{\lambda\alpha}W_1 \tag{18}$$

where W_1, W_2, and W_3 are the derivatives of W with respect to its first, second, and third variables. At the surface of stress discontinuities $r = a_1, a_2, b, c$, the associated tractions need to be equal but opposite, which requires the radial stress to be continuous across r, that is

$$\begin{aligned} T_{rr}(a_1^+) &= T_{rr}(a_1^-), \qquad T_{rr}(a_2^+) = T_{rr}(a_2^-), \\ T_{rr}(b^+) &= T_{rr}(b^-), \qquad T_{rr}(c^+) = T_{rr}(c^-). \end{aligned} \tag{19}$$

For an internal pressure P, the two free parameters a and λ are obtained by solving simultaneously the axial equilibrium and boundary condition

$$T_{rr}(d) = 0, \qquad \int_a^d rT_{zz}(r)dr = \pi a^2 P. \tag{20}$$

The stress in a system will depend on the geometry. Therefore, when studying the effect of residual stress, it will be important to compare two structures with the same dimensions where one has residual stress and one does not. In this case, the grown dimensions of the load-free cylinder are pre-determined and the free parameter is the initial inner radii, A, instead of the grown inner radii, a. Based on experimental data by [1], the dimensions in the current (grown) configuration are set to $a = 1.0$ mm, $a_1 = 1.15$ mm, $a_2 = 1.69$ mm, $b = 1.89$ mm, $c = 1.97$ mm, and $d = 2.02$ mm.

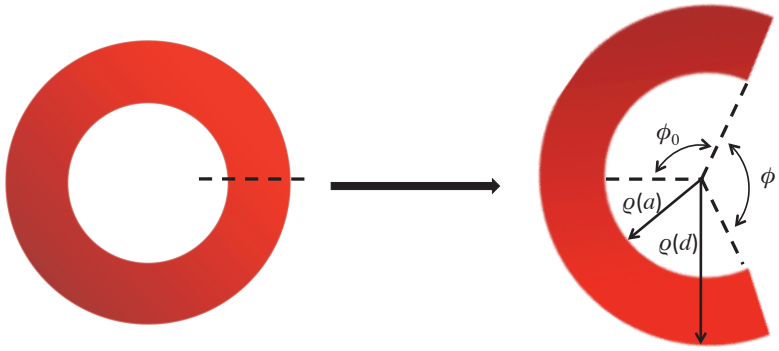

FIGURE 3. Schematic of a radial cut in an artery and the corresponding opening angle ϕ.

2.6. **Residual stress.** The form of the growth tensor can be determined by ensuring compatibility with a given residual stress field. [10] separated the layers of an artery and measured the change in length. Using this data, the axial growth is assumed to be $\gamma_z = 1.14$ in both the intima and necrotic layers, $\gamma_z = 1.05$ in the media, and $\gamma_z = 1$ in the adventitia. To determine the radial growth, we use data on the opening angle from a radial cut on a thin ring of artery, as done by [31]. The basic idea is to consider an additional decomposition from configuration $\mathcal{V}$ to $\mathcal{B}_f$. The material elements in the configuration $\mathcal{V}$ are reassembled into the configuration $\mathcal{B}_1$, which represents a single opened ring due to a radial cut (Figure 1). The deformation $\mathbf{A}_a$ to configuration $\mathcal{B}_1$ will contain residual stress if the elements of $\mathcal{V}$ are geometrically incompatible. Lastly, the deformation $\mathbf{A}_b$ bends the ring closed and the ring is subjected to an internal pressure P to produce the final configuration $\mathcal{B}_f$.

The cylindrical polar coordinates in $\mathcal{B}_1$ are given by (ρ, ϑ, ζ). The elastic tensor $\mathbf{A}$ can be decomposed into the product of two tensors, $\mathbf{A} = \mathbf{A}_a \cdot \mathbf{A}_b$, where

$$\mathbf{A}_a = \operatorname{diag}(\alpha_{a\rho}, \alpha_{a\vartheta}, \alpha_{a\zeta}), \qquad \mathbf{A}_b = \operatorname{diag}(\alpha_{b\rho}, \alpha_{b\vartheta}, \alpha_{b\zeta}). \tag{21}$$

The solution for configuration $\mathcal{B}_f$ is calculated as described in Section 2.5. Once this solution is known, the geometry and corresponding stresses in the cut ring can be determined as follows. The total deformation in terms of the material coordinates in $\mathcal{B}_1$ is given by

$$r = r(\rho), \quad \theta = \pi\vartheta/\varphi_0, \quad z = \Lambda\zeta, \tag{22}$$

where Λ is the axial stretch and φ_0 is the angle related to the opening angle $\varphi = 2(\pi - \varphi_0)$ defined in Figure 3. The kinematic relationships are given by

$$\alpha_{a\rho} = \lambda_r(\alpha_{b\rho}\gamma_r)^{-1}, \quad \alpha_{a\vartheta} = \lambda_\theta(\alpha_{b\vartheta}\gamma_\theta)^{-1}, \quad \alpha_{az} = \lambda_z(\alpha_{b\zeta}\gamma_z)^{-1}, \tag{23}$$

$$\alpha_{b\rho} = \partial r/\partial\rho, \quad \alpha_{b\vartheta} = \pi r/\varphi_0\rho, \quad \alpha_{b\zeta} = \Lambda, \tag{24}$$

and the incompressibility conditions are given by

$$\alpha_{a\rho}\alpha_{a\vartheta}\alpha_{az} = \alpha_{b\rho}\alpha_{b\vartheta}\alpha_{bz} = 1. \tag{25}$$

The equilibrium equation is

$$\frac{\partial T_{\rho\rho}}{\partial\rho} + \frac{T_{\rho\rho} - T_{\vartheta\vartheta}}{\rho} = 0, \tag{26}$$

where the Cauchy stress components T_{ii} in $\mathcal{B}_1$ are given by

$$T_{ii} = \alpha_{ai}\frac{\partial W}{\partial\alpha_{ai}} - \hat{p}. \tag{27}$$

The subscript i corresponds to the parameters ρ,ϑ,and ζ, $\hat{p}$ is the Lagrange multiplier in $\mathcal{B}_1$, and the strain-energy density function is $W = W(\alpha_{a\rho}, \alpha_{a\vartheta}, \alpha_\zeta)$. In the unloaded configuration $\mathcal{B}_1$, we assume zero net axial force and bending moment and zero normal traction on the inner and outer boundaries,

$$\int_{\rho(a)}^{\rho(d)} T_{\zeta\zeta}\rho d\rho = 0, \quad \int_{\rho(a)}^{\rho(d)} T_{\vartheta\vartheta}\rho d\rho = 0, \tag{28}$$

$$T_{\rho\rho}[\rho(a)] = T_{\rho\rho}[\rho(d)] = 0, \tag{29}$$

where $\rho(a)$ and $\rho(d)$ are the inner and outer radii in $\mathcal{B}_1$.

Substituting the expressions from (24) into the incompressibility condition (25) yields

$$\frac{\pi\Lambda r}{\varphi_0\rho}\frac{\partial r}{\partial\rho} = 1, \tag{30}$$

which can be integrated to obtain

$$\rho(r) = \left(\rho(a)^2 + \frac{\pi\Lambda}{\varphi_0}(r^2 - a^2)\right)^{1/2}. \tag{31}$$

Equations (28) can be written in terms of the material cooordinate r by using the relationship in (30),

$$\frac{\pi\Lambda}{\varphi_0}\int_a^d rT_{\zeta\zeta}(r)dr = 0, \qquad \frac{\pi\Lambda}{\varphi 0}\int_a^d rT_{\vartheta\vartheta}(r)dr = 0. \tag{32}$$

The equilibrium equation (26) is integrated to obtain an equation for the radial stress

$$T_{\rho\rho}(r) = \frac{\pi\Lambda}{\varphi_0}\int_a^r \frac{r}{\rho(r)^2}(T_{\vartheta\vartheta}(r) - T_{\rho\rho}(r))dr. \tag{33}$$

Substituting the boundary condition at the outer boundary ($T_{\rho\rho}(d) = 0$) into the previous equation yields

$$\frac{\pi\Lambda}{\varphi_0}\int_a^d \left(\frac{r}{\rho(r)^2}(T_{\vartheta\vartheta}(r) - T_{\rho\rho}(r)\right)dr = 0. \tag{34}$$

Equations (32) and (34) are used to solve for the unknown parameters $\rho(a)$, Λ, and φ_0 and the solution for $\mathcal{B}_1$ is completely determined. The opening angle of human coronary arteries can vary depending on the degree of arteriosclerosis and distance from the right coronary artery orifice. Based on data from [36], the opening angle is

assumed to be 130 °. The radial growth corresponding to an opening angle of 130 ° is $\gamma_r = 1.326$ where the radial growth is assumed to be the same in each layer.

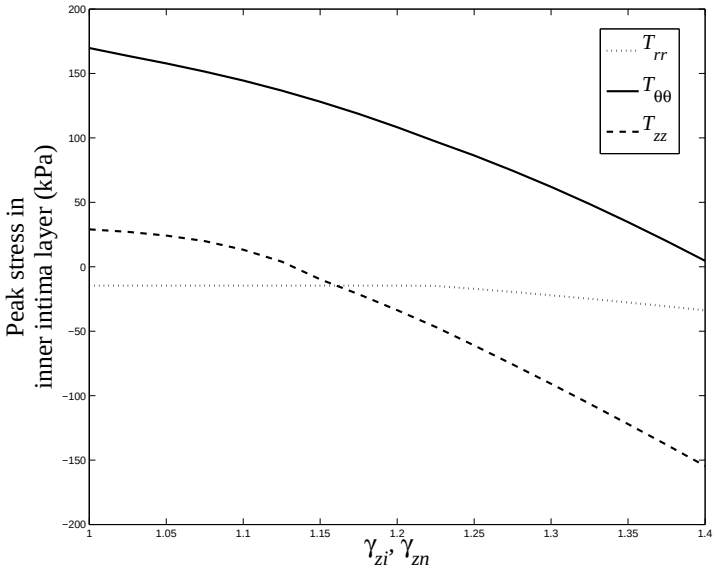

FIGURE 4. Effect of γ_z on the peak stress in the inner intima layer.

3. **Results.** High stress can occur in the thin cap of an atherosclerotic artery which may lead to rupture. Therefore, it is imperative to understand what affects the stress distribution in the inner intima layer. Using the baseline parameter values denoted in Table 1, we vary particular values to study the effects of morphological and mechanical features on the stress in the inner intima layer. Furthermore, we investigate the importance of including residual stress in the calculation.

3.1. **Effect of residual stress.** As noted in the introduction, most studies have neglected residual stress when calculating stress distributions in arteries. Residual stress is introduced through differential growth. Therefore, we study how axial and radial growth affect the peak stress. First we consider the effect of differential growth in the axial direction by varying γ_z in the intima and necrotic layers. The peak stresses in the radial, circumferential and axial directions in the inner intima layer are plotted with respect to γ_z in Figure 4. Note that the peak stress is defined as the stress with largest absolute value. The radial stress is compressive, hoop stress is tensile, and axial stress changes from tensile to compressive as the axial growth increases. For low growth values, the maximum stress is in the circumferential direction. Increasing γ_z between 1 and 1.2740 results in a decrease in peak stress by 56%. As γ_z increases past 1.2740, the difference in growth in the layers causes the peak stress to be in the axial direction. This stress increases as γ_z increases. However, physiologically reasonable values of γ_z are in the region where the peak stress is in the circumferential direction.

Symbol	Meaning	Value	Reference
γ_{zi}, γ_{zn}	axial growth in intima/necrotic	1.14	[10]
γ_{zm}	axial growth in media	1.05	[10]
γ_{za}	axial growth in adventitia	1	[10]
γ_{ri}, γ_{rn}, γ_{rm}, γ_{ra}	radial growth in each layer	1.326	Eq. (32), (34), [36]
μ_m	stress-like parameter	1.27	[11]
μ_a	stress-like parameter	7.56	[11]
k_{1m}	stress-like parameter	21.60	[11]
k_{1a}	stress-like parameter	38.57	[11]
k_{2m}	non-dimensional parameter	8.21	[11]
k_{2a}	non-dimensional parameter	85.03	[11]
ρ_m	non-dimensional parameter	0.25	[11]
ρ_a	non-dimensional parameter	0.55	[11]
ϕ_m	angle between fibers	20.61°	[11]
ϕ_a	angle between fibers	67°	[11]
E_i	intima Young's modulus	$100 - 1000$ kPa	[4], [15], [3], [14]
E_n	necrotic Young's modulus	1 kPa	[19]
P	internal pressure	14.6 kPa	-
a	grown lumen radius	1.0 mm	[1]
a_1	grown intima-necrotic radius	1.15 mm	[1]
a_2	grown necrotic-intima radius	1.69 mm	[1]
b	grown intima-media radius	1.89 mm	[1]
c	grown media-adventitia radius	1.97 mm	[1]
d	grown outer wall radius	2.02 mm	[1]

TABLE 1. Parameters and their baseline numerical values.

Very little data exists on estimates of axial stress in arteries. However, an experiment on human aortas with non-atherosclerotic intimal thickening show that the media and adventitia are in tension in the intact artery and the intima is in compression [10]. Based on their length measurements after separating the layers of arteries, axial growth in our model is given by $\gamma_z = 1.14$ in the intima and necrotic layers, $\gamma_z = 1.05$ in the media, and $\gamma_z = 1$ in the adventitia. Using these values for axial growth, the effect of radial growth on the peak stress is considered. It is assumed there is no growth in the circumferential direction and γ_r is the same for each layer. Figure 5 shows that the circumferential peak stress initially increases as γ_r is increased and then it decreases. Varying γ_r has a large effect on the peak stress. Based on our estimate of the radial growth found in Section 2.6 ($\gamma_r = 1.326$), we see that the peak stress occurs in the circumferential direction. Because we know that the peak stress occurs in the circumferential direction, wee will denote the peak cap stress as PCS .

3.2. **Effect of low stiffness layer.** A study by [24] showed that the size of the necrotic core has a significant influence on stresses in the inner intima layer. However, their model does not incorporate residual stress. The effects of the thickness of the necrotic layer are shown in Figure 6 for an artery with residual stress and without residual stress. The peak cap stress (PCS) is plotted versus the thickness of the necrotic layer. The geometry of the artery without residual stress before

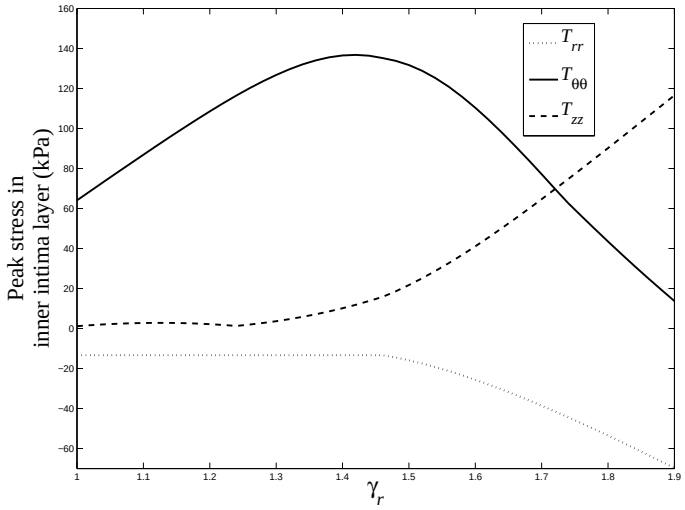

FIGURE 5. Effect of γ_{rj} for $j = i, n, m, a$ on the peak stress in the inner intima layer.

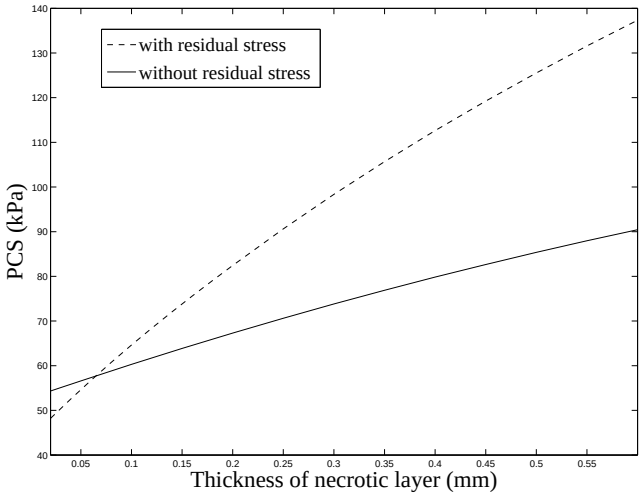

FIGURE 6. Effect of necrotic layer thickness on peak stress.

an internal pressure is applied is identical to the grown artery with residual stress. Therefore, geometrical effects do not account for the differences in peak stresses that are observed. The residual stress increases the peak stress in the inner intima layer except in the case of a very thin necrotic layer. In addition, a residually stressed artery would produce a larger increase in peak stress when doubling the thickness of the necrotic layer. For example, suppose the thickness of the necrotic layer is 0.27 mm. Compared to an artery with a necrotic layer of 0.54 mm, the residually

stressed artery results in a 39% increase in peak stress whereas the peak stress in the artery without residual stress increases by only 21.6%. The baseline estimate for the necrotic layer thickness is 0.54 mm. At this value, the residually stressed artery has a much higher PCS.

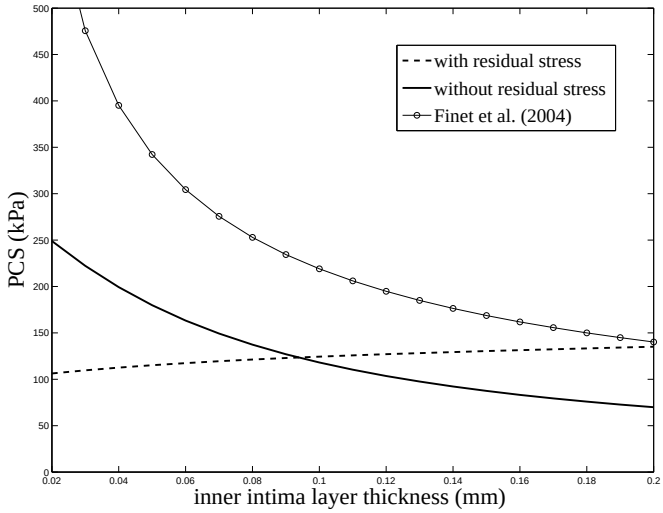

FIGURE 7. Effect of cap thickness on peak stress.

3.3. **Effect of inner intima layer thickness.** [6] used a computational structural analysis based on three typical in-vivo intravascular ultrasound images of fibrous cap atheroma to study the effect of decreasing the cap thickness (CTh). In three plaques studied, the mean curve interpolation of the three curves PCS versus CTh is given by

$$PCS = 49.72 * CTh^{-0.644} \tag{35}$$

where cap thickness is in mm and PCS is in kPa. Residual stress was not included in their model and the plaques were eccentric. Estimates of PCS from other studies are seen in Table 2. The estimate in [6] is plotted along with our model results in Figure 7. The artery without residual stress displays similar behavior as the model in [6]. The peak stress increases as the cap thickness decreases in an artery with no residual stress. However, the opposite is true for a residually stressed structure. Furthermore, for small cap thicknesses, the residually stressed artery has a much lower peak stress.

Peak Stress	Reference
$67 - 364$ kPa	[19]
$385 - 705$ kPa	[37]
$126.4 - 238.2$ kPa	[22]

TABLE 2. Peak stress computed using finite element analysis in eccentric plaques.

3.4. **Effect of outer intima layer thickness.** Figure 8 shows the effect of the outer intima layer thickness on the peak stress. The peak stress in an artery without residual stress will decrease as the thickness of the layer increases. On the other hand, when residual stress is present the peak stress increases. However, the peak stress changes very little over a wide range of thicknesses in the residually stressed artery.

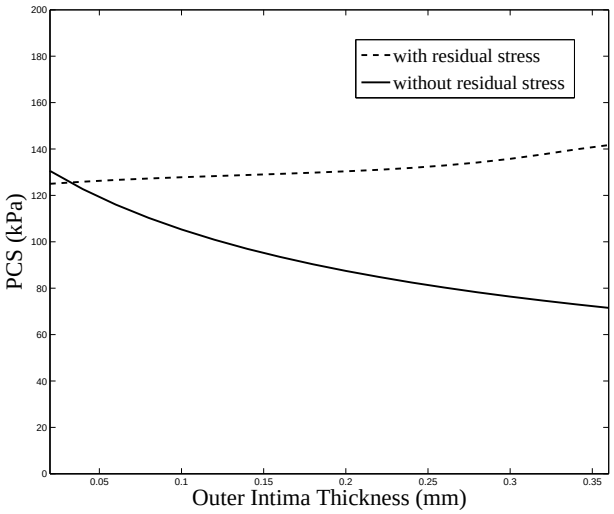

FIGURE 8. Effect of thickness of outer intima layer on peak stress.

3.5. **Effect of intima stiffness.** As discussed in Section 2.3, the stiffness of the intima can vary greatly. For a residually stressed vessel, Figure 9 shows the peak stress versus cap layer thickness for various stiffness values. The necrotic layer has very low stiffness. Therefore, when the intima is very stiff, it will support a higher stress no matter the cap thickness. For low stiffness, the stresses are more evenly distributed across the layers and the peak stress in the cap is lower than the other cases. Also note that the peak stress decreases as a function of cap thickness only if the intima stiffness is below a particular threshold.

4. **Conclusion.** Understanding the stress distributions in the wall of an atheroslcerotic artery and how morphological and mechanical features affect these stresses is crucial to understand the risk of plaque rupture ([6], [19], [24]). However, residual stresses are largely ignored in structural analyses and therefore the effects of residual stress on atherosclerotic artery walls is not well understood. Therefore, in this study, a simple geometry was used to better understand the role of residual stress on peak stress in the inner intima layer. In this paper we have considered a mechanical model of arteries that includes a stiff intima and a necrotic layer with low stiffness. The necrotic layer was characterized as a soft, neo-Hookean material and the cap had identical material properties as the intima layer behind the necrotic layer. The model of [11] was used for the mechanical part of the media and adventitia, and the approach of [28] was used for the modeling of residual stress. Residual stress is

introduced through differential growth of the artery layers. The form of the growth tensor was found by matching theoretical results to opening angle experiments.

Studies have shown that stresses in the cap increase with decreasing cap thickness ([6], [33], [19]). Our model agrees with this result for an artery without residual stress. However, decreasing cap thickness can actually decrease the peak cap stress when residual stress is included and the intima is stiff. [24] showed that the size of the necrotic core has a significant influence on cap stresses. We also observe this influence in our model but we also see that as the thickness of the necrotic layer increases, the peak stress in the residually stress cylinder increases at a greater rate than the cylinder without residual stress.

Finite element analyses performed by [2] showed that cap thickness was the most important morphological risk factor for stiff intima models in stiff intima models. Here, the influence of the inner and outer intima layers was shown to have a large effect in the case of a vessel without residual stress. However, the peak stress changed very little as the thickness of the intima layers varied in a residually stressed vessel. The thickness of the necrotic layer had a large effect on the peak stress in a vessel with residual stress. Overall, in the residually stressed cylinder, the thickness of the low stiffness layer played the largest role in affecting the peak stress.

This study strengthens the importance of residual stress in calculating stress distributions in atherosclerotic arteries. Furthermore, axial residual stress in particular clearly plays an important role and therefore a three-dimensional model is important in capturing these effects. The complex interactions of growth and stress can result in counter-intuitive results and it is important to carefully study the effects of differential growth and residual stress. A model that uses a non-axisymmetric geometry would be needed to next study how geometry affects the overall stress distribution. These results could then be compared to experimental data on the material strength of various layers to describe the risk of rupture in the vessel.

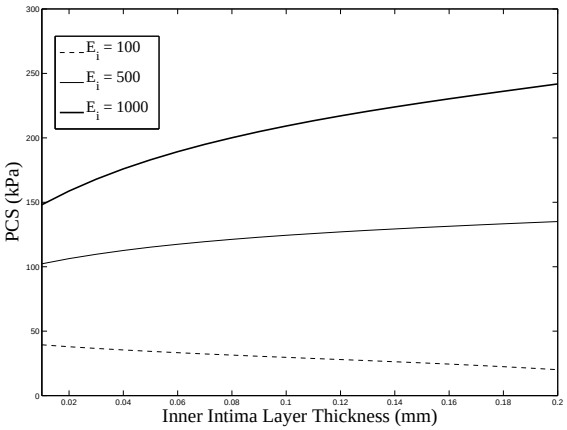

FIGURE 9. Peak cap stress plotted with respect to the thickness of cap for different values of the intima stiffness.

REFERENCES

[1] A. Akyildiz, L. Speelman, H. Nieuwstadt, S. J. W. Van Der and F. Gijsen, Influence of plaque geometry on peak cap stress, *Proceedings of the ASME 2011 Summer Bioegnineering ConferenceArtery Research*, **5** (2011), 159–160.

[2] A. Akyildiz, L. Speelman, H. van Brummelen, M. Gutiérrez, R. Virmani, A. van der Lugt, A. Van Der Steen, J. Wentzel and F. Gijsen, Effects of intima stiffness and plaque morphology on peak cap stress, *Biomedical Engineering Online*, **10** (2011), 1–13.

[3] R. Baldewsing, C. De Korte, J. Schaar, F. Mastik and Van Der Steen, Finite element modeling and intravascular ultrasound elastography of vulnerable plaques: Parameter variation, *Ultrasonics*, **42** (2004), 723–729.

[4] S. Barrett, M. Sutcliffe, S. Howarth, Z. Li and J. Gillard, Experimental measurement of the mechanical properties of carotid atherothrombotic plaque fibrous cap, *Journal of Biomechanics*, **42** (2009), 1650–1655.

[5] E. Falk, K. S. Prediman and F. Valenin, Coronary Plaque Disruption, *Circulation*, **92** (1995), 657–671.

[6] G. Finet, J. Ohayon and G. Rioufol, Biomechanical interaction between cap thickness, lipid core composition and blood pressure in vulnerable coronary plaque: Impact on stability or instability, *Coronary artery disease*, **15** (2004), 13–20.

[7] A. Goriely and R. Vandiver, On the mechanical stability of growing arteries, *IMA Journal of Applied Mathematics*, **75** (2010), 549–570.

[8] G. Holzapfel, *Nonlinear Solid Mechanics: A Continuum Approach for Engineering*, John Wiley & Sons Ltd. 2000.

[9] G. Holzapfel, T. Gasser and R. Ogden, Comparison of a multi-layer structural model for arterial walls with a Fung-type model, and issues of material stability, *Journal of Biomechanical Engineering*, **126** (2004), 264–275.

[10] G. Holzapfel, G. Sommer, M. Auer, P. Regitnig and R. Ogden, Layer-specific 3D residual deformations of human aortas with non-atherosclerotic intimal thickening, *Annals of Biomedical Engineering*, **35** (2007), 530–545.

[11] G. Holzapfel, G. Sommer, C. Gasser and P. Regitnig, Determination of layer-specific mechanical properties of human coronary arteries with nonatherosclerotic intimal thickening and related constitutive modeling, *American Journal of Physiology-Heart and Circulatory Physiology*, **289** (2005), H2048–H2058.

[12] P. Kalita and R. Schaefer, Mechanical models of artery walls, *Archives of Computational Methods in Engineering*, **15** (2008), 1–36.

[13] E. Lee, Elastic-plastic deformation at finite strains, *J. Appl. Mech.*, **36** (1968), 1–6.

[14] R. Lee, A. Grodzinsky, E. Frank, R. Kamm and F. Schoen, Structure-dependent dynamic mechanical behavior of fibrous caps from human atherosclerotic plaques, *Circulation*, **83** (1991), 1764–1770.

[15] R. Lee, S. Richardson, H. Loree, A. Grodzinsky, S. Gharib, F. Schoen and N. Pandian, Prediction of mechanical properties of human atherosclerotic tissue by high-frequency intravascular ultrasound imaging. An in vitro study, *Arteriosclerosis, Thrombosis, and Vascular Biology*, **12** (1992), 1–5.

[16] M. Li, J. Beech-Brandt, L. John, P. Hoskins and W. Easson, Numerical analysis of pulsatile blood flow and vessel wall mechanics in different degrees of stenoses, *Journal of Biomechanics*, **40** (2007), 3715–3724.

[17] A. Li, S. Howarth and R. Trivedi, Stress analysis of carotid plaque rupture based on in vivo high resolution MRI, *Journal of Biomechanics*, **39** (2006), 2611–2622.

[18] S. Liu and Y. Fung, Zero-stress states of arteries, *Journal of Biomechanical Engineering*, **110** (1988), 82–84.

[19] H. Loree, R. Kamm, R. Stringfellow and R. Lee, Effects of fibrous cap thickness on peak circumferential stress in model atherosclerotic vessels, *Circulation research*, **71** (1992), 850–858.

[20] H. Loree, B. Tobias, L. Gibson, R. Kamm, D. Small and R. Lee, Mechanical properties of model atherosclerotic lesion lipid pools, *Arteriosclerosis, Thrombosis, and Vascular Biology*, **14** (1994), 230–234.

[21] M. Naghavi, P. Libby, E. Falk, S. Casscells, S. Litovsky, J. Rumberger, J. Badimon, C. Stefanadis, P. Moreno and P. Pasterkamp, From vulnerable plaque to vulnerable patient a

call for new definitions and risk assessment strategies: Part I, *Circulation*, **108** (2003), 1664–1672.

[22] J. Ohayon, N. Mesnler, A. Brolsat, J. Toczek, L. Rlou and Pl Tracqui, Elucidating atherosclerotic vulnerable plaque rupture by modeling cross substitution of ApoE mouse and human plaque components stiffnesses, *Biomech. Model. Mechanobiol.*, **11** (2011), 801–813.

[23] J. Ohayon, O. Dubreuil, P. Tracqui, S. Le Floc'h, G. Rioufol, L. Chalabreysse, F. Thivolet, R. Pettigrew and G. Finet, Influence of residual stress/strain on the biomechanical stability of vulnerable coronary plaques: Potential impact for evaluating the risk of plaque rupture, *American Journal of Physiology-Heart and Circulatory Physiology*, **293** (2007), H1987–H1996.

[24] J. Ohayon, G. Finet, A. Gharib, D. Herzka, P. Tracqui, J. Heroux, G. Rioufol, M. Kotys, A. Elagha and R. Pettigrew, Necrotic core thickness and positive arterial remodeling index: Emergent biomechanical factors for evaluating the risk of plaque rupture, *American Journal of Physiology-Heart and Circulatory Physiology*, **295** (2008), H717–H727.

[25] A. Rachev, Theoretical study of the effect of stress-dependent remodeling on arterial geometry under hypertensive conditions, *Journal of Biomechanics*, **30** (1997), 819–827.

[26] E. Rodriguez, A. Hoger and A. McCulloch, Stress-dependent finite growth in soft elastic tissues, *Journal of Biomechanics*, **27** (1994), 455–467.

[27] U. Sadat, Z. Teng and J. Gillard, Biomechanical structural stresses of atherosclerotic plaques, *Expert Review of Cardiovascular Therapy*, **8** (2010), 1469–1481.

[28] L. Taber, Biomechanical growth laws for muscle tissue, *Journal of Theoretical Biology*, **193** (1998), 201–213.

[29] L. Taber, A model for aortic growth based on fluid shear and fiber stresses, *Journal of Biomechanical Engineering*, **120** (1998), 348–354.

[30] L. Taber and D. Eggers, Theoretical study of stress-modulated growth in the aorta, *Journal of Theoretical Biology*, **180** (1996), 343–357.

[31] L. Taber and J. Humphrey, Stress-modulated growth, residual stress, and vascular heterogeneity, *Journal of Biomechanical Engineering*, **123** (2001), 528–535.

[32] D. Tang, Z. Teng, G. Canton, C. Yang, M. Ferguson, X. Huang, J. Zheng, P. Woodard and C. Yuan, Sites of rupture in human atherosclerotic carotid plaques are associated with high structural stresses, *Stroke*, **40** (2009), 3258–3263.

[33] D. Tang, C. Yang, J. Zheng, P. Woodard, G. Sicard, J. Saffitz and C. Yuan, 3D MRI-based multicomponent FSI models for atherosclerotic plaques, *Annals of Biomedical Engineering*, **32** (2004), 947–960.

[34] Z. Teng, G. Canton, C. Yuan, M. Ferguson, C. Yang, X. Huang, J. Zheng, P. Woodard and D. Tang, 3D critical plaque wall stress is a better predictor of carotid plaque rupture sites than flow shear stress: An in vivo MRI-based 3D FSI study, *Journal of Biomechanical Engineering*, **132** (2010), 031007.

[35] R. Vaishnav and J. Vossoughi, Residual stress and strain in aortic segments, *Journal of Biomechanics*, **20** (1987), 235–237.

[36] J. Valenta, J. Svoboda, D. Valerianova and K. Vitek, Residual strain in human atherosclerotic coronary arteries and age related geometrical changes, *Biomedical Materials and Engineering*, **9** (1999), 311–318.

[37] Y. Vengrenyuk, S. Carlier, S. Xanthos, L. Cardos, P. Ganatos, R. Virmani, S. Einav, L. Gilchrist and S. Weinbaum, A hypothesis for vulnerable plaque rupture due to stress-induced debonding around cellular microcalcifications in thin fibrous caps, *PNAS*, **103** (2006), 14678–14683.

Received January 31, 2014; Accepted April 01, 2014.

E-mail address: vandiver@stolaf.edu